Supplemental Materials

Molecular Biology of the Cell

Pantazopoulou et al.

Supplemental Figure S1. *rabE* is an essential gene
(A) Colonies of a *pyrG89* strain transformed with the linearized *rabE*Δ*::pyrG*^{Af} construct were streaked on medium supplemented or not with pyrimidines. Colonies marked HK#1, 2 and 3 are heterokaryons that do not growth on selective pyrimidine-less medium. DI#1 and 2 are diploid strains that grow on both media and serve as internal control (these strains also demonstrate that the deletion allele is recessive). Note that the two colonies magnified (2x) in the inset show arborescent growth typical of heterokaryons (compare their tree-like growth and conidiation with those of control diploid strains), which further confirms that the deletion allele can be only maintained in heterokaryosis (see also scheme in Figure 1A); (This residual heterokaryotic growth results from a carry over of heterokaryotic mycelium with the conidiospore suspension used to inoculate these plates). (B) Terminal phenotype of *rabE*Δ*::pyrG*^{Af} . Spores of an untransformed *pyrG89* control strain (top panel) did not establish polarity. However, a proportion of spores obtained from heterokaryotic transformants established polarity (they thus represent *rabE*Δ*::pyrG*^{Af} pyrimidine prototrophs) but were unable to maintain it, arresting with a 'large bud phenotype', indicating that the *rabE*Δ*::pyrG*^{Af}*::*allele segregates into conidiospores and that it is essentially lethal. (C) PCR genotyping of the *rabE*$^{+}$ and *rabE*Δ*::pyrG*^{Af} alleles in heterokaryotic and diploid transformants. (D) *rabD*Δ*::pyrG*^{Af} transformants show impaired conidiation but grow in the absence of pyrimidine supplementation. (E) Southern analysis demonstrating that *rabD*Δ*::pyrG*^{Af} transformants show the expected gene replacement event. (F) *rabD*Δ*::pyrG*^{Af} conidia are able to establish and maintain polarity, although hyphae are wider than normal.

Supplemental Figure S2. Fluorescent protein-tagged constructs and expression levels
(A) Scheme of the genomic organization of the *rabE* locus in strain MAD4120 and derivatives. This strain still has the resident *rabE* gene, in addition to carrying a GFP-*rabE* gene driven by the natural *rabE* promoter integrated at the *rabE* locus. (B) The growth phenotype of the GFP-tagged gene replacement allele. A linear DNA fragment was used to replace the resident *rabE* gene. Comparison of strains resulting from cross-overs 2 an 3 (in which the replaced *rabE* gene is untagged) with those resulting from cross-overs 1 and 3 (thus GFP-tagged) showed that GFP tagging leads to detectable growth impairment. (C) RabE and GFP-RabE protein levels as determined by anti-RabE western blotting in the indicated strains. The gene-replaced strain is MAD4055. Note that levels of the GFP-tagged protein are ~3.5 times lower than those of the untagged one, encoded by the endogenous allele, indicating that GFP tagging reduces the steady-state levels of the protein. (D) Anti-GFP western blotting analysis showing the different GFP-RabE levels driven by *alcA*^{p} on different carbon sources. A replicate reacted with α-actin antibody serves as loading control. The scheme shows that the transgene is targeted in single copy to the *argB* locus (strain MAD3069). (E) Steady-state levels of mCherry-RabE driven by *alcA*^{p} on different carbon sources, as determined with α-RabE antiserum. Note that levels on fructose (two different concentrations tested) are lower than the endogenous levels. Ethanol results in overexpression. The scheme shows that the transgene is targeted in single copy to the *argB* locus. Strain MAD3575. (A, B, D, E) All microscopy images shown below the corresponding transgene in inverted greyscale are at the same magnification.

Supplemental Figure S3. Maturation of LGC into post-Golgi carriers monitored with HypB^{Sec7}
(A) Example of dual-channel imaging of HypB^{Sec7}–GFP and mCherry-RabE^{RAB11}. HypB^{Sec7}-GFP was expressed after endogenous tagging, whereas mCherry-RabE^{RAB11} expression was driven by *alcA*^{p}, using fructose as carbon source, which results in similar fluorescence in the mCherry and GFP channels, enabling image acquisition with a Dual-View

beam splitter. Experiment carried out with strain MAD5098. (B) Kymographs of GFP-HypB^{Sec7} and mCherry-RabE^{RAB11} channels derived from time-series constructed with projections of Z-stacks acquired every 3.3 sec and deconvolved. Left, the insets in the GFP and mCherry channels are shown merged, at double magnification. Strain and conditions were as in (A). (C) Quantitation of GFP-HypB^{Sec7} and mCherry-RabE^{RAB11} channels for n=7 cisternae maturing into post-Golgi RabE^{RAB11} carriers. (D) Example of one of these events with quantitation of the two channels.

Supplemental Figure S4. The abnormal *hypB5* aggregate of RabE^{RAB11} membranes also contains RabA^{RAB5}.

Colocalization of GFP-RabE and mCherry-RabA in a *hypB*5 cell, following a 50 min shift to a restrictive temperature. Under such conditions RabE^{RAB11} is present in abnormal membrane aggregates, and this experiment shows that in these there is detectable colocalization with the early endosomal marker mCherry-RabA. It should be emphasized that in wild-type cells RabA early endosomes and RabE carriers are distinct populations (Supplemental Figure S6 and S7) and thus that this colocalization of the two Rabs is caused by the abnormal membrane traffic resulting from HypB^{Sec7} impairment. Inverted greyscale images represent maximal intensity projections of Z-stacks, whereas colored images represent optical sections (Z-pass indicated). This experiment was carried out with strain MAD5078, using fructose as carbon source. Control experiments with strain MAD5082 demonstrated that abnormal RabE^{RAB11} aggregates also form in *hypB*5 cells that do not express mCherry-RabA (not shown). All images are at the same magnification.

Supplemental Figure S5. MT organization controls and effect of benomyl on RabE^{RAB11} carriers

(A) TubA-GFP labeled microtubules in the tip regions of cells with the indicated genetic backgrounds, or in the presence of the also indicated cytoskeletal inhibitors. Images are projections of Z-stacks treated with the 'unsharp' filter of Metamorph, to enhance contrast. All panels are shown at the same magnification (*myoE*Δ cells are conspicuously wider than the wild-type). (B) Kymographs of GFP-RabE carriers in wild-type hyphal tips treated or not with benomyl. Note that benomyl results in complete MT depolymerization [panel (A)].

Supplemental Figure S6. RabE^{RAB11} carriers and RabA^{RAB5} early endosomes are distinct populations

(A) Kymograph capturing trajectories of RabA^{RAB5}-labeled early endosomes and GFP-RabE carriers. They were derived from movies in which the red and green channels were photographed simultaneously using a Dual-View beam splitter. (B) As above in a cell treated with latrunculin B to displace SPK RabE^{RAB11} carriers to the MT conveyor belt. (C) GFP-RabE and mCherry-RabA aggregated in different structures in cells treated with both latrunculin B and benomyl.

Supplemental Figure S7. RabE^{RAB11} carriers and PdnIns3P endosomes are distinct populations

Non-overlapping trajectories of GFP-FYVE$_2$-labeled early endosomes and mCherry-RabE carriers captured with kymographs (strain MAD5072). These were derived from movies in which the red and green channels were photographed simultaneously using a Dual-View beam splitter. Kymographs corresponding to a tip-proximal region (where RabE^{RAB11} carriers are most abundant) and a tip-distal region are shown. In either case RabE^{RAB11} carriers are more abundant than early endosomes labeled with GFP-FYVE$_2$.

Supplemental Figure S8 RabE^{RAB11} and mRFP-PH^{OSBP} localize to static aggregates in a hyphal tip cell treated with both latB and benomyl
The pictures display a hyphal tip cell treated with both latB and benomyl for 28 min. Images represent the starting frame of a time-stack acquisition (71 frames, 1 frame every 3 sec) in which each time frame is a maximal intensity projection of a Z-stack. The kymograph at the bottom shows that GFP-RabE and mRFP-PH^{OSBP} aggregates do not overlap over time.

Supplemental Table S1
A. nidulans strains used in this work

Supplemental Table S2
Oligonucleotides used for genetic manipulation and diagnostic PCRs

Supplemental Movie S1
GFP-RabE carriers arriving at the prominent SPK in a cell undergoing apical extension. The GFP channel is shown in inverted grey scale. Strain MAD4120. Time is in min:sec:msec.

Supplemental Movie S2
mCherry-RabE colocalizing with MyoE-GFP in the SPK of several hyphae growing over a ~ 30 min period. Strain MAD4403 cultured on fructose. Time is in h:min:sec

Supplemental Movie S3
Late Golgi cisternae labeled with mRFP-PH^{OSBP} mature into GFP-RabE post-Golgi carriers over time. These carriers are delivered to the SPK. Individual frames represent maximal intensity projections of deconvolved z-stacks of strain MAD4440 (1 stack every 4 sec). Time is in min:sec.

Supplemental Movie S4
Late Golgi cisternae labeled with mRFP-PH^{OSBP} co-filmed with GFP-RabE with a time resolution of 250 msec. The boxed region contains two LGC captured during their transition to RabE^{RAB11} carriers that subsequently undergo movement towards the SPK. Frames represent middle planes of strain MAD4440. Time is in sec:msec

Supplemental Movie S5
Late Golgi cisternae labeled with HypB^{Sec7}-GFP co-filmed with mCherry-RabE. Individual frames represent maximal intensity projections of deconvolved Z-stacks of strain MAD5098 (1 stack every 3.3 sec). An example of a LGC that forms after 9 sec and matures into a RabE carrier is arrowed in the corresponding channels. Time is in min:sec.

Supplemental Movie S6
GFP-RabE carriers following trajectories of TubA-GFP MTs. An example of one such carrier moving to the SPK is indicated with a grey arrowhead. Strain MAD4263. Time is in sec:msec.

Supplemental Movie S7
Movie highlighting one example of a GFP-RabE carrier (grey arrowhead) that moves basipetally within the tip region, following the trajectory of a TubA-GFP MT in strain MAD4263. Time is in sec:msec

Supplemental Movie S8
Rapidly moving GFP-RabE structures in a hyphal tip of strain MAD4120 cell treated with latB. Time is in sec:msec

Supplemental Movie S9
GFP-RabE structures rapidly moving on the MT conveyor belt in latB-treated MAD4263 cell that co-expresses GFP-labeled TubA to reveal the position of the MTs. Time is in sec:msec.

Supplemental Movie S10
GFP-RabE carriers arriving at the characteristic apical crescents of several *myoE*Δ hyphal tip cells. Strain MAD4409. Time is in sec:msec.

Supplemental Movie S11
Two parallel sequences with the same time resolution of GFP-RabE carriers showing decoration of actin cables in a *myoE*Δ tip (top sequence) alongside with a benomyl-treated *myoE*Δ tip (bottom). Note the complete absence of moving structures and actin cable decoration in the bottom sequence. Strain MAD4409. Time in sec:msec.

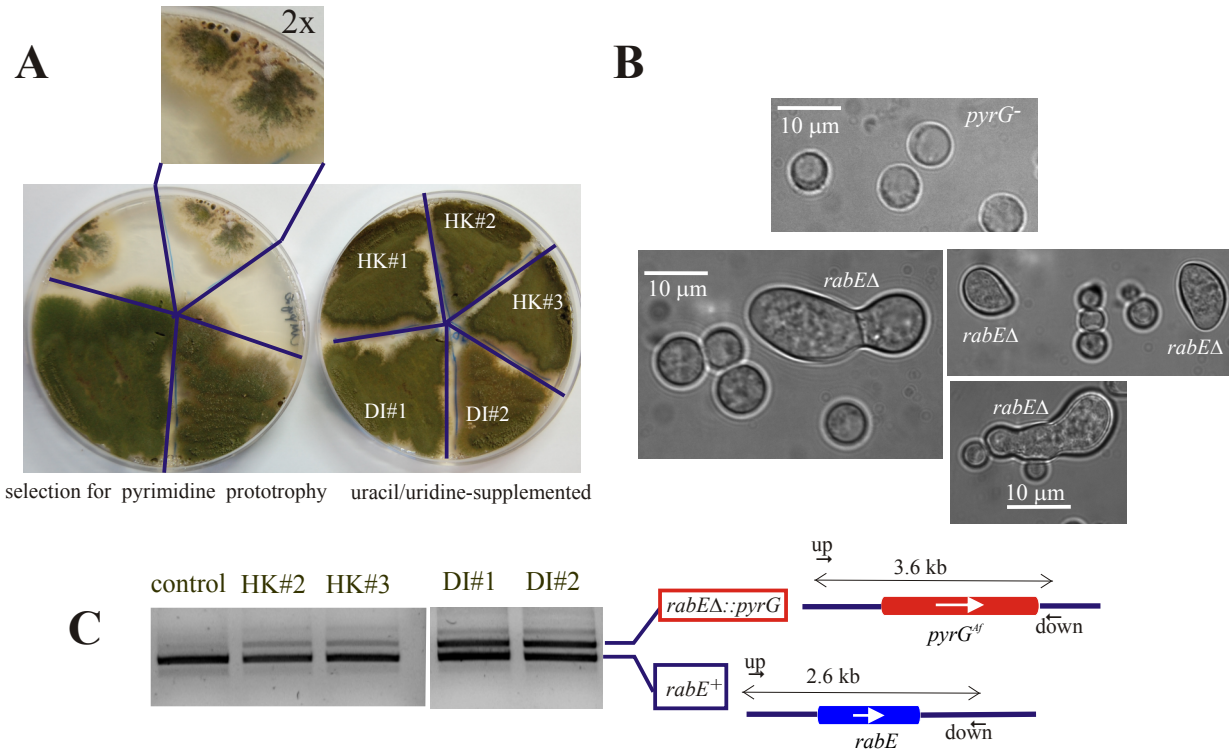

Supplemental Figure S1

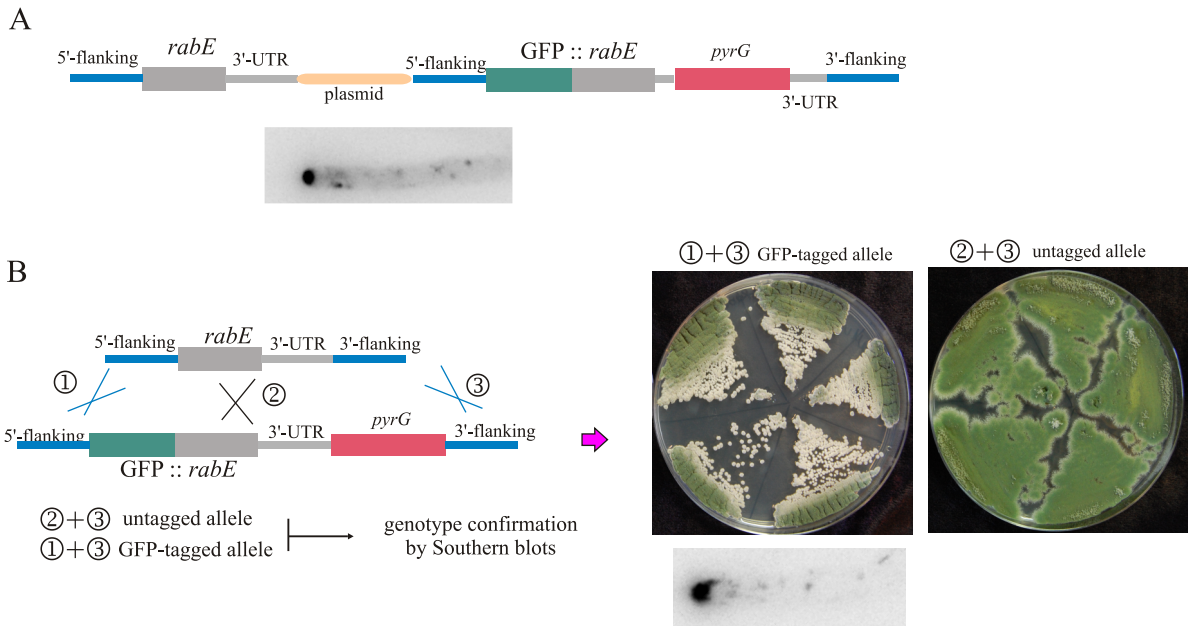

Supplemental Figure S2

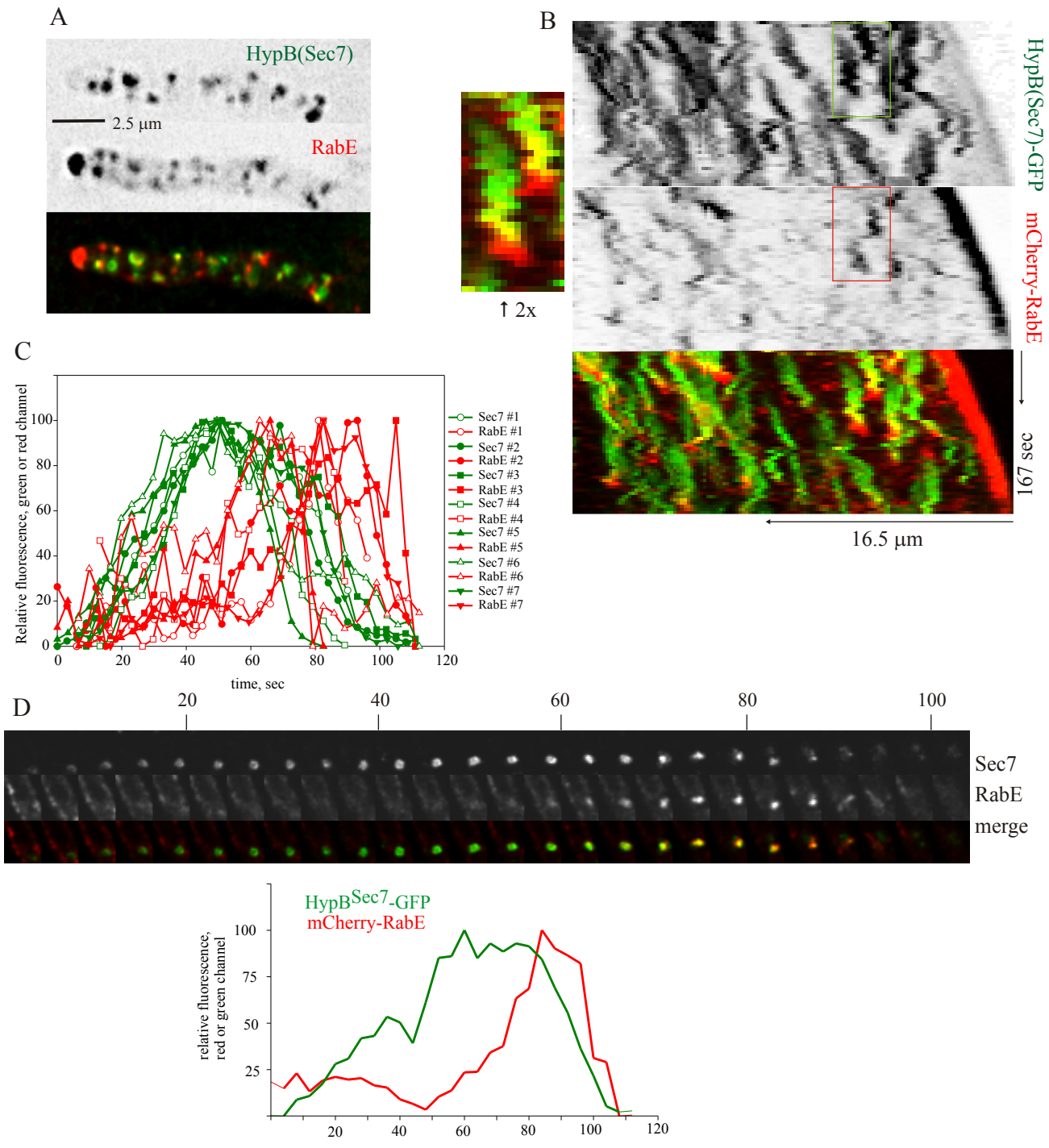

Supplemental Figure S3

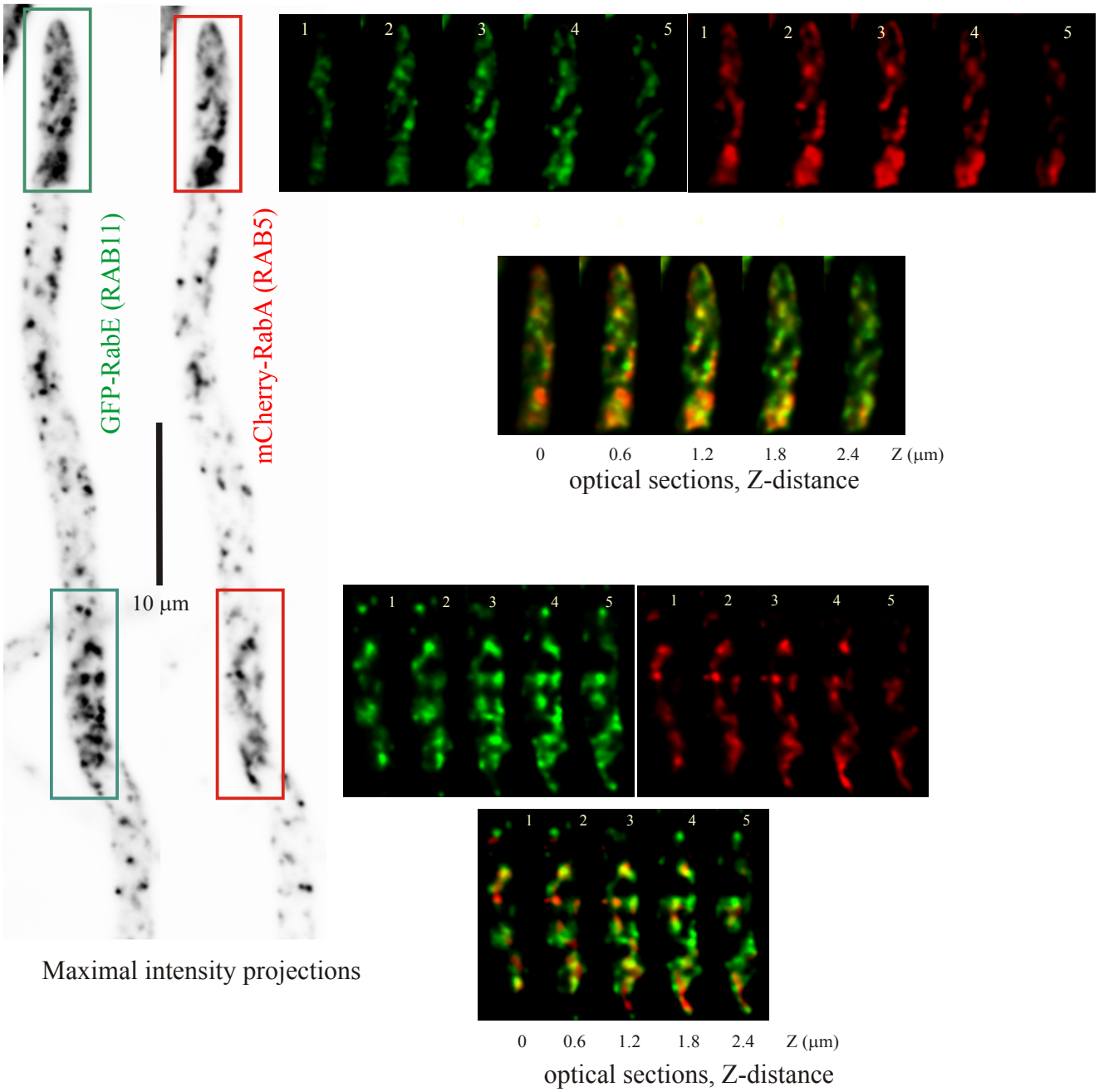

Maximal intensity projections

Supplemental Figure S4

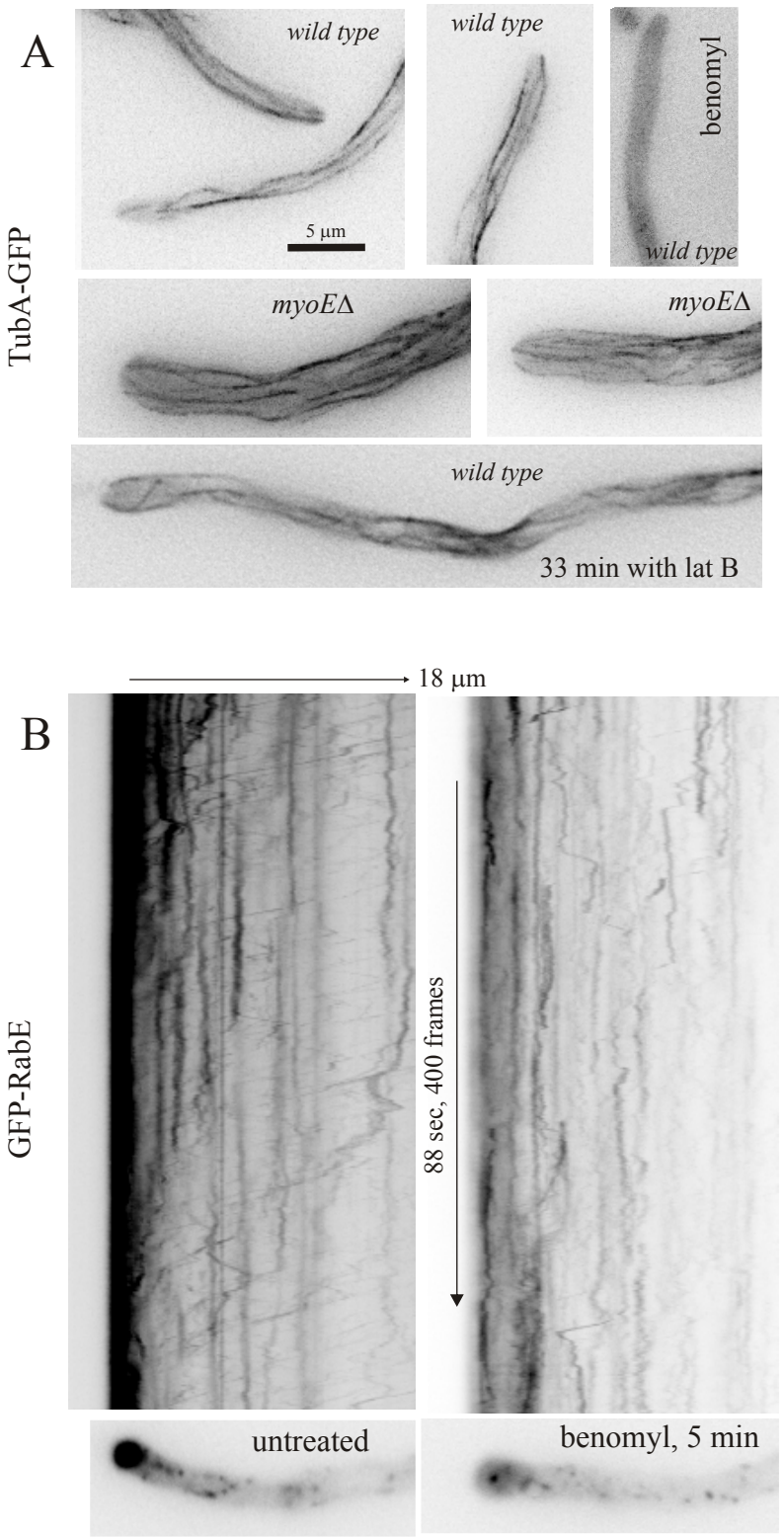

Supplemental Figure S5

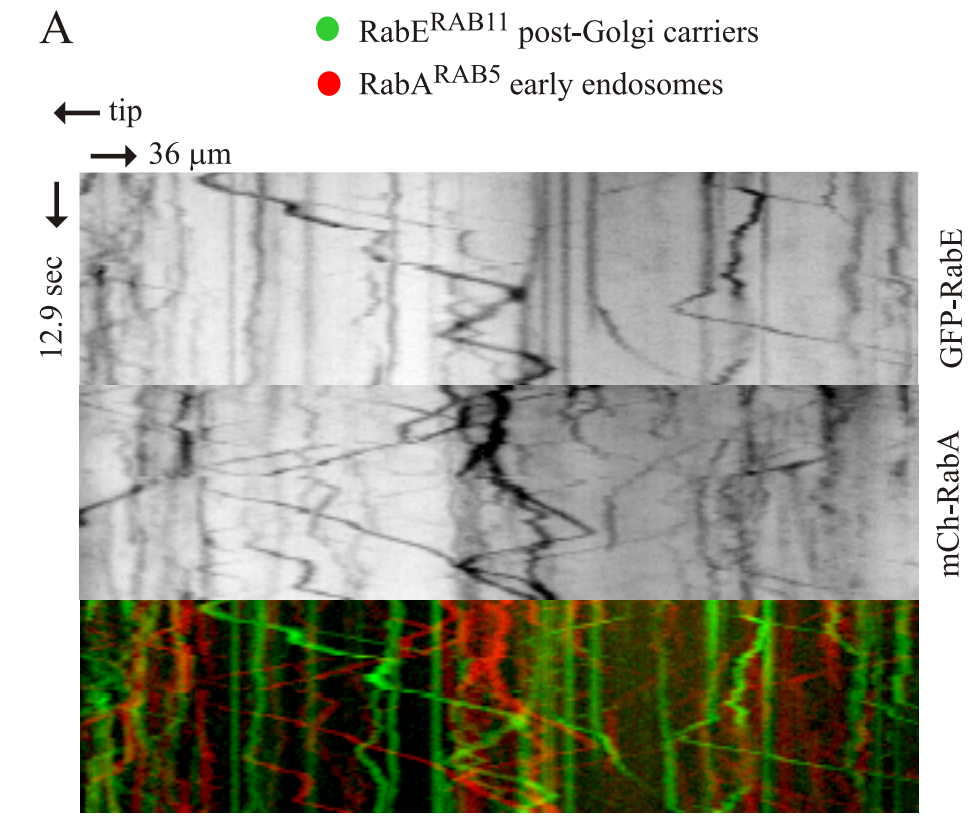

untreated cell, subapical region

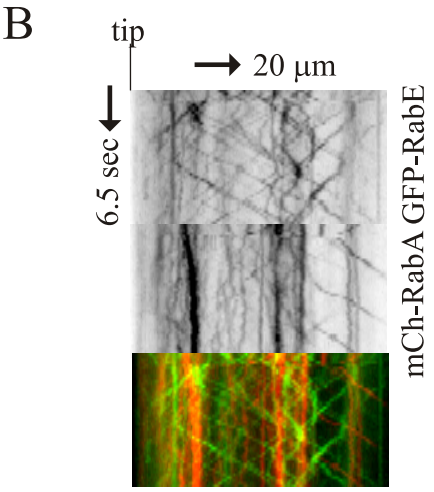

hyphal cell treated with latB

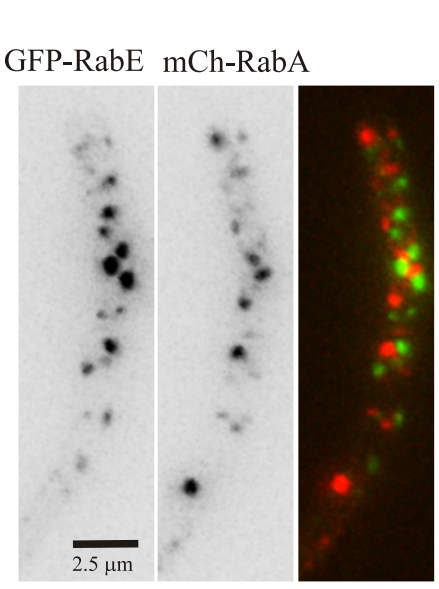

hyphal tip cell treated with both lat B and benomyl

Supplemental Figure S6

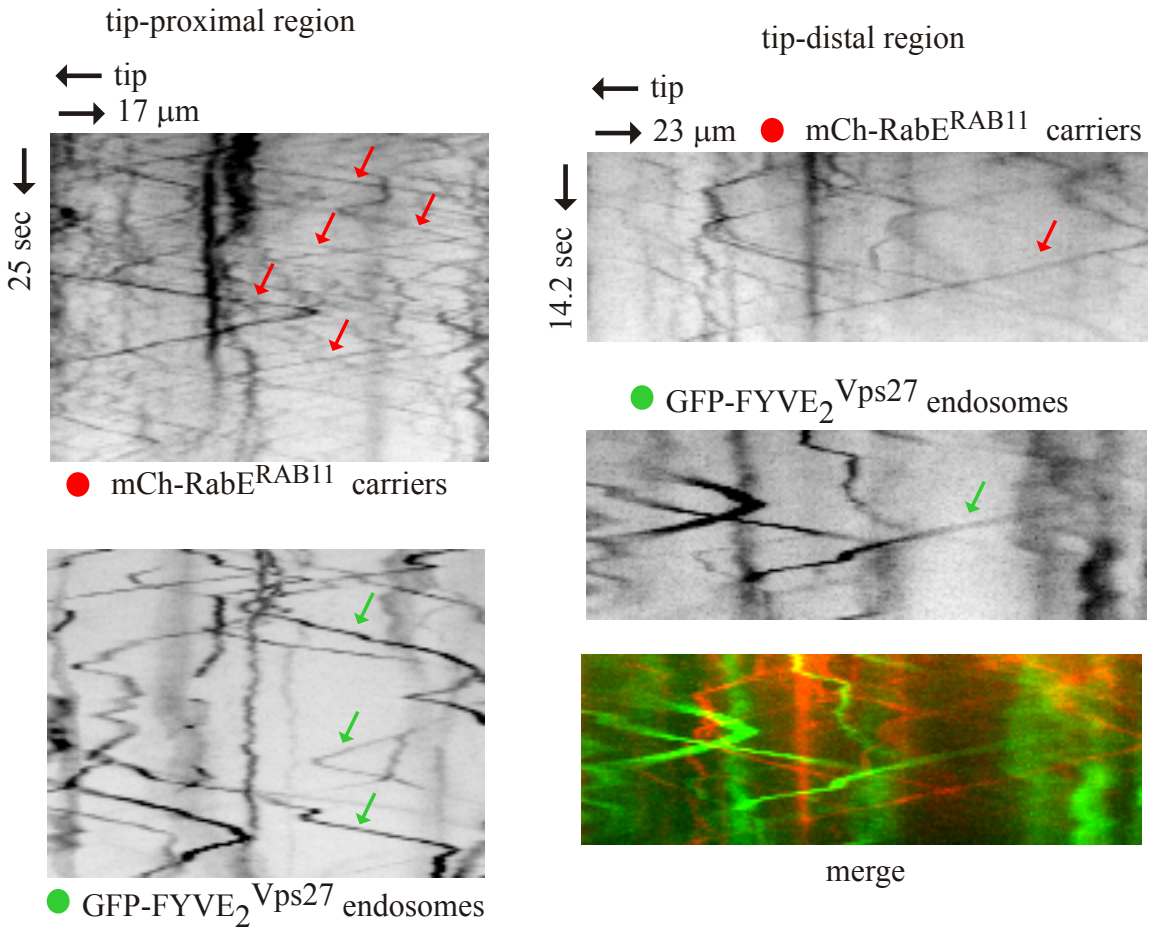

Supplemental Figure S7

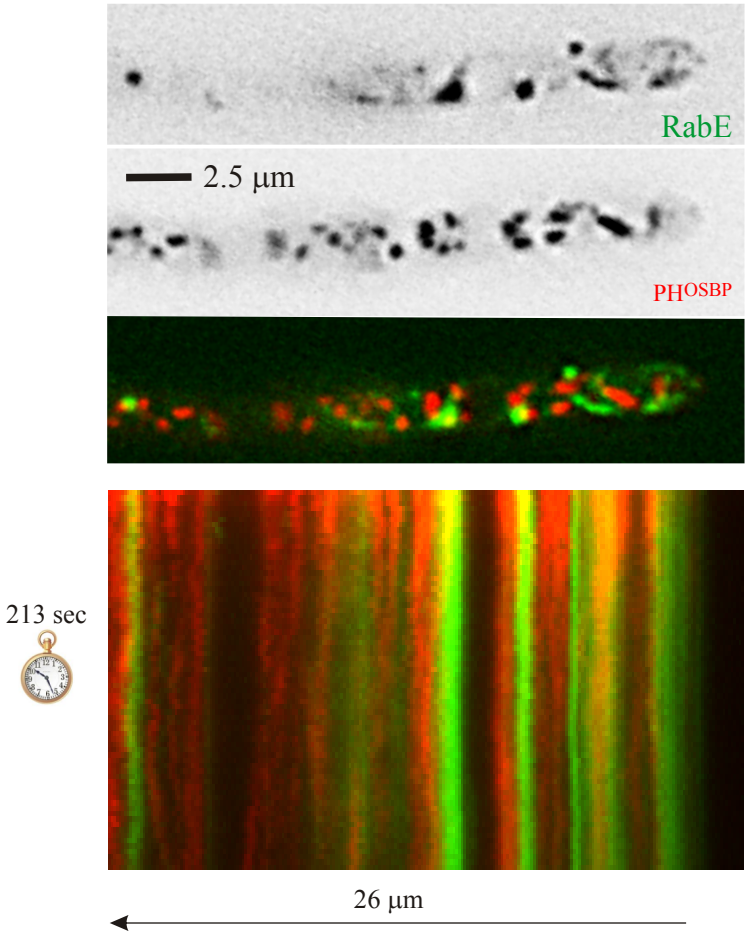

Supplemental Figure S8

Table S1 *A. nidulans* strains used in this work

MAD number[*1]	Genotype	Source
540	*pabaA1 yA2; argB2 (glc-)*	Nowak B
1117	*yA2; argB2; pantoB100*	Espeso E
1739	*pyrG89; nkuAΔ::bar pyroA4*	Arst HN
1741	*wA4; inoB2 nkuAΔ::bar pyroA4; niiA4*	Arst HN
1750	*pyrG89; wA3; pyroA4; tpmA::gfp::pyr4*	(Pearson CL et al, 2004)
2013	*wA4; inoB2 nkuAΔ::bar pyroA4 [pyroA*-gpdA^{mini}::mrfp::PH^{OSBP}]; niiA4*	(Pantazopoulou and Peñalva, 2009)
2023	*pyrG89; sc12; choA1; chaA1 tubA::gfp*	Oakley B
2262	*pabaA1; pantoB100*	Abenza JF
2275	*yA2; argB2[argB*-alcAp::mCherry::rabA]; pantoB100*	(Abenza et al, 2009)
2523	*biA1 hypB5 pabaA6; chaA1*	(Yang et al, 2008)
3069	*pabaA1 yA2; argB2[argB*-alcA^{p}::gfp::rabE]*	This work
3167	*yA2; argB2[argB*-alcA^{p}::gfp::rabE]; inoB2 nkuAΔ::bar? pyroA4 [pyro*-gpdA^{mini}::mrfp::PH^{OSBP}]; niiA4*	This work
3320	*biA1 pabaA6 pyrG89?; synA^{p}::synA::gfp::pyrG^{Af}; nkuAΔ::bar?*	This work
3323	*biA1 hypB5 pabaA6 pyrG89?; synA^{p}::synA::gfp::pyrG^{Af} ; nkuAΔ::bar*	(Pinar et al, 2013b)
3575	*pabaA1 yA2; argB2[argB*-alcA^{p}::mcherry::rabE]*	This work
3584	*pyrG89; nkuAΔ::bar pyroA4 rabDΔ::pyrG^{Af}*	This work
3632	*hypB5; argB2[argB*-alcA^{p}::gfp::rabE]; nkuAΔ::bar? pyroA4 [pyroA*-gpdA^{mini}::mrfp::PH^{OSBP}]*	This work
4033	*wA4; inoB2 nkuAΔ::bar pyroA4[pyroA*-alcA^{p}::gfp::rabD]; niiA4*	This work
4055	*pyrG89; pyroA4 nkuAΔ::bar; [rabE^{p}::gfp::rabE::pyrG^{Af}]*	This work
4072	*pabaA1 yA2; , argB2[argB*-alcAp::gfp::ypt31]; inoB2*	This work
4120	*pyrG89; pyroA4 nkuAΔ::bar; [rabE^{p}::rabE::rabE^{p}::gfp::rabE::pyrG^{Af}]*	This work
4156	*argB2 [argB*-alcA^{p}::mcherry::rabE]; inoB2 nkuAΔ::bar? pyroA4[pyroA*-alcA^{p}::gfp::rabD]; niiA4*	This work
4220	*yA2 pyrG89?; argB2(argB*-alcA^{p}::mcherry::RabA], nkuAΔ::bar? pyroA4; [rabE^{p}::rabE::rabEp::gfp::rabE::pyrG^{Af}]*	This work
4225	*yA2 pyrG89?; nkuAΔ::bar?; pantoB100 [rabE^{p}::rabE::rabE^{p}::gfp::rabE::pyrG^{Af}]*	This work
4263	*pyrG89; nkuAΔ?; choA1; tubAgfp [rabE^{p}::rabE::rabE^{p}::gfp::rabE::pyrG^{Af}]*	This work
4271	*yA2; argB2(argB*-alcA^{p}::gfp::S23NrabE); pantoB100*	This work

4370	*pyrG89; myoEΔ::pyrG^{Af}; nkuAΔ::argB pyroA4 ; riboB2*	(Taheri-Talesh N et al, 2012)
4371	*pyrG89; myoE::gfp::pyrG^{Af}; nkuAΔ::argB pyroA4; nicA2; fwA1*	(Taheri-Talesh N et al, 2012)
4403	*pabaA1 pyrG89?; argB2[argB*-alcA^{p}::mcherry::rabE] myoE::gfp::pyrG^{Af}; nkuAD::bar? pyroA4; fwA1*	This work
4409	*pyrG89?; myoEΔ::pyrG^{Af}; nkuAΔ::argB?; [rabE^{p}::rabE::rabE^{p}::gfp::rabE::pyrG^{Af}]*	This work
4440	*pyrG89?; nkuAΔ::bar pyroA4[pyroA*-gpdA^{mini}::mrfp::PH^{OSBP}], [rabE^{p}::rabE::rabE^{p}::gfp::rabE::pyrG^{Af}]*	This work
4658	*pyrG89; wA::gfp::tubA::pyrG^{Af}, nkuAΔ::argB pyroA4*	Oakley Berl
4824	*pyrG89; wA::gfp::tubA::pyrG^{Af}, myoEΔ::pyrG^{Af}; nkuAΔ::argB? pyroA4*	This work
4859	*hypA1 pyrG89?; nkuAΔ::bar? pyroA4; [rabE^{p}::rabE::rabE^{p}::gfp::rabE::pyrG^{Af}]*	This work
5072	*yA2?; wA4; argB2::[argB*-alcA^{p}::mCherry-RabE]; pyroA4::*[*pyroA*-alcA^{p}*::(*vps27-FYVE*)$_2$::*gfp*]; *nkuAΔ::bar?; niiA4*	This work
5078	*hypB5 yA2 pyrG89?; argB2::[argB*-alcAp::mcherry::RabA]; nkuAΔ::bar? [rabE^{p}::rabE::rabE^{p}::gfp::rabE::pyrG^{Af}]*	This work
5082	*hypB5 pyrG89?; nkuAΔ::bar?; [rabE^{p}::rabE::rabE^{p}::gfp::rabE::pyrG^{Af}]*	This work
5098	*hypB::gfp::pyrG^{Af} pyrG89?; argB2[argB*-alcA^{p}::mcherry::rabE]; pyroA4 nkuAΔ::bar?*	This work

[*1] *Strain numeration refers to their assigned number in the MAD (Madrid, CIB-CSIC) collection*

Table S2 Oligonucleotides used for genetic manipulation and diagnostic PCRs

Primer list number	Primer name	Sequence 5´-3´
1	Fw BamHI RabE	CGTGGATCCATGGCTAACGAC
2	RevXhoIRabE	CGGCTCGAGTTAACAGCATCCACCCTTGTTC
3	FWBamHIGFP	CCGGGATCCATGAGTAAAGGAGAAGAAC
4	Rev GFP-GA BamHI	CATGGATCCGGCACCGGCTCCAGCGC
5	RabE S23N Fw	CGATAGTGGAACGGGAAAGAACAATCTGCTATCGCGTTTTACC
6	RabE S23N Rev	GGTAAAACGCGATAGCAGATTGTTCTTTCCCGTTCCACTATCG
7	Fw 5UTR RabE	CCTTGCCTTCGGCAATTCGC
8	Rev 5UTR RabE	GCGAACAGTTAGATACACCG
9	FW joint 5UTRRabE GFP	CCCTCGGTGTATCTAACTGTTCGCTATGAGTAAAGGAGAAGAACTT
10	Fw joint RabEORF-pyrG	GGGTGGATGCTGTTAACTCGAGCCGACCGGTCGCCTCAAACAATGCTCTTC
11	Rev Join 3UTRRabE-pyrG	GGCCAGAACCGCAAATCGTTGTTGACCTGTCTGAGAGGAGGCACTGATGCG
12	Fw 3UTR RabE	GTCAACAACGATTTGCGGTTC
13	Rev 3UTR RabE	GGGTTATGTAATCACCTGCGG
14	FwJoin5UTRRabE-pyrG	CTCCCTCGGTGTATCTAACTGTTCGCACCGGTCGCCTCAAACAATGCTCTTC
15	Fw 5UTR RabD	CGAAAGCTCTGTTAGACGCG
16	Rev 5UTR RabD	GTGAGCAAATTTCTTTGCGATC
17	Fw join 5UTR RabD pyrG	CTATCAGATCGCAAAGAAATTTGCTCACACCGGTCGCCTCAAACAATGCTCTTC
18	Rev join 3UTR RabD pyrG	GTATGAAGAATGGCACATAATGTATTCACTGTCTGAGAGGAGGCACTGATGCG
19	Fw 3UTR RabD	TGAATACATTATGTGCCATTCTTC
20	Rev 3UTR RabD	CTGAAGCCAAATAGAGATG
21	Rev EcoRI GA6	GGGGAATTCGGCACCGGCTCCAGCGCC
22	Fw EcoRI RabD	GGGGAATTCATGGCTGGCACTAGAAACTATGAC
23	Rev XmaI RabD	AAACCCGGGTCAACAACACTTTCCTCCGGC